東京大学大学院新領域創成科学研究科

先端生命科学専攻

2024 年度

修士論文

液胞リン脂質分解酵素 Atg15 の膜認識特異性の研究

Studies of Membrane Recognition Specificity of Vacuolar Phospholipase Atg15

生命応答システム分野

学籍番号:47-236310

氏名:岡田脩平

2024 年 12 月提出

指導教員　鈴木邦律　准教授

Table of contents

List of Tables

List of Figures

Abbreviations

ALPS	·····	Amphipathic lipid packing sensor
Ape1	·····	Aminopeptidase I
Atg	·····	Autophagy-related
BAR	·····	Bin/Amphiphysin/Rvs
CD	·····	Circular dichroism
CtAtg15	·····	*Chaetomium thermophilum* Atg15
Cvt	·····	Cytoplasm-to-vacuole targeting
DIC	·····	Differential interference contrast
GUV	·····	Giant unilamellar vesicle
PtdCho	·····	Phosphatidylcholine
PtdIns	·····	Phosphatidylinositol
PtdSer	·····	Phosphatidylserine
MVB	·····	Multi vesicular body
ScAtg15	·····	*Saccharomyces cerevisiae* Atg15
TCA	·····	Trichloroacetic acid
TMD	·····	Transmembrane domain

Abstract

Atg15 (autophagy-related 15), a vacuolar phospholipase, plays a crucial role in the degradation of membranes of organelles transported into the vacuole, such as autophagic bodies and mitochondria, enabling the recycling of cellular components. However, despite the activity within the vacuolar lumen, Atg15 does not disrupt the vacuolar limiting membrane. This study investigates the mechanism by which Atg15 recognizes substrate membranes, primarily focusing on the relationship between membrane curvature and the affinity of Atg15 for membranes. My findings reveal a correlation between membrane curvature and the affinity of Atg15 for membranes, suggesting that Atg15 preferentially recognizes membranes with high positive curvature, which may explain the resistance of the vacuolar limiting membrane against Atg15. Additionally, CD spectra analysis suggests that Atg15 undergoes structural changes with increased flexibility under acidic pH, which may correlate with its substrate selectivity. I also demonstrated that the basic amino acid residues proximal to the active center are essential for the enzymatic activity of Atg15 but do not contribute to the substrate recognition. These findings provide insights into how Atg15 recognizes its substrates and how vacuole membranes avoid digestion by Atg15.

Introduction

Macroautophagy (hereafter called “autophagy”) is a well-conserved intracellular degradation system among eukaryotic cells from yeast to mammals (Mizushima et al., 2011). When autophagy is induced in *Saccharomyces cerevisiae*, Atg proteins are recruited near the vacuolar membrane and form the pre-autophagosomal structure (PAS). The PAS is separated from the cytoplasm through liquid-liquid phase separation, formed through interactions among the proteins that constitute the PAS. Further downstream Atg proteins are recruited to the PAS, then a membrane sac called the isolation membrane (IM) is generated. The IM expands while encapsulating cytoplasmic materials such as proteins and organelles, eventually closes to form an autophagosome, a double-membrane organelle to isolate them. The outer membrane of the autophagosome is then fused with vacuole, the lytic compartment in a yeast cell (lysosomes in mammals) to release the inner membrane. A vesicle composed of the inner membrane is called the autophagic body (AB), and the limiting membrane of the AB is degraded by lipase, followed by the degradation of its contents by hydrolase in a vacuole. Through these series of steps, the degradation of intracellular components by autophagy is completed (Fig. 1; Takeshige et al., 1992).

Atg15 is a glycosylated membrane protein that contains motifs conserved in esterases and lipases, and it is essential for the degradation of ABs in *S. cerevisiae* (Epple et al., 2001; Teter et al., 2001). After its translation, Atg15 is transported to the vacuole via the MVB pathway, dependent on its N-terminal transmembrane domain, and directs the predicted lipase domain at the C-terminal region to the vacuolar lumen (Hirata et al., 2021). Recent studies have experimentally confirmed that the C-terminal domain of Atg15 functions as a phospholipase that degrades phospholipids (Kagohashi et al., 2023; Watanabe et al., 2023). It was previously reported that the membrane disruption of ABs depends on Atg15 and the vacuolar protease Pep4 (Epple et al., 2001). Meanwhile, research by Watanabe et al. using Atg15 of the thermophilic fungus *Chaetomium thermophilum* (CtAtg15) revealed that the lipase domain of CtAtg15 undergoes cleavage by a protease. This cleavage induces structural changes around the catalytic site, resulting in the shift in a loop (S243–S253) and a short helix (S404–G408), along with the shortening an α-helix (S179–S193), exposing the active center S330. Consequently, this structural rearrangement produces an open active state and significantly enhances lipase activity.

These studies have shown that Atg15 directly degrades the membranes of ABs and mitochondria inside ABs (Kagohashi et al., 2023; Watanabe et al., 2023). Additionally, other

research has shown that in cells undergoing lipophagy, the degradation of lipid droplet proteins depends on Atg15 (van Zutphen et al., 2013). Similarly, during rapamycin-induced autophagy of peroxisomes, the degradation of peroxisomal proteins also relies on Atg15 (Boutouja et al., 2019). Furthermore, in the process of Piecemeal Microautophagy of the Nucleus (PMN), which selectively removes and degrades small fragments of the nucleus, small vesicles characterized by the nuclear membrane accumulated in a vacuole in Atg15 deficient cells (Millen et al., 2009). These results indicate that Atg15 degrades not only the membranes of ABs but also those of other organelles transported into the vacuole.

Recent studies have begun to shed light on the functions and regulation of Atg15. However, a remaining mystery about the vacuolar lipase Atg15 is that, although it is activated in the vacuolar lumen and degrades the membranes of vesicles transported to the vacuole, it does not degrade the vacuolar limiting membrane. The vacuolar membrane is a lipid membrane rich in phospholipids, which are thought to be substrates for Atg15. In microautophagy, the substrates are encapsulated by vacuolar membranes and incorporated into a vacuole. Indeed, it was suggested that PMNs-derived vesicles were degraded by Atg15 (Millen et al., 2009), implying that vacuolar membranes incorporated into the vacuolar lumen, along with other organelle membranes, may also be targeted by Atg15. This raises the question: what prevents Atg15 from degrading the vacuolar limiting membrane? Although experimental evidence on Atg15 is limited, several possible hypotheses have been proposed. One of the hypotheses is that Atg15 is unable to degrade membranes with negative curvature. Vesicles within the vacuolar lumen exhibit positive curvature from the viewpoint from Atg15 within the vacuolar lumen, whereas the vacuolar membrane presents negative curvature. In general, higher membrane curvature results in looser lipid packing, while lower curvature leads to tighter packing. Looser lipid packing increases the spacing between lipid head groups in lipid bilayers and causing the hydrophobic region of the membrane to become more exposed at the surface. Atg15 exhibits phospholipase B activity, hydrolyzing the acyl chains at the sn-1 and sn-2 positions of the glycerol backbone in phospholipids (Watanabe et al., 2023). This targeted ester bond resides near the hydrophobic region of lipid bilayers, suggesting that some degree of lipid packing defect may be necessary for Atg15 to access it. While there are other hypotheses, in this study, I primarily focuses on examining how Atg15 activity changes in response to the curvature of substrate membranes. By investigating the nature of the membrane binding affinity of Atg15, I hope to provide insights into why vacuolar membranes are not degraded by Atg15. For this purpose, I utilized Atg15 of the thermophilic fungus *C. thermophilum*, following the approach

reported by our group (Watanabe et al., 2023).

Results

Acid Conditions Enhanced Liposome Binding and Degradation by CtAtg15

In a previous study, CtAtg15 was shown to exhibit the highest activity in degrading phospholipids in micells at pH 4.0 (Watanabe et al., 2023). Given that ABs and organelles transported to the vacuole are more similar to liposomes than to micelles, I investigated the activity of CtAtg15 against liposomes across different pH levels. For this experiment, I used the recombinant lipase domain of CtAtg15 (CtAtg15 (73-475)). Specifically, 5 μM CtAtg15(73-475) was incubated with 2 mM liposomes (DOPC/DOPE/NBD-PE: 50/30/10) and 4.5 μM proteinase K at 30°C for indicated times. After incubation, the organic layer was extracted using an established method (Bligh and Dyer, 1959) and separated by TLC, revealing three distinct spots Mass spectrometry analysis identified the middle spots as NBD-PE, while the other two spots were shown to result from the degradation of NBD-PE, with the spots migrating the farthest corresponding to NBD-FFA and the spots migrating the least corresponding to NBD-lysoPE (Watanabe et al., 2023). The NBD-FFA and NBD-lysoPE spots indicate the degradative activity of CtAtg15 on NBD-PE. As a result, signals of NBD-lysoPE and NBD-FFA were most strongly detected at pH 4.0, with weakly detected at pH 3.1 and pH 5.0, and minimal at pH 6.0 (Fig. 2A).

Next, I examined the binding affinity of CtAtg15 to liposomes at each pH. In this experiment, I used S330A mutant form of the lipase domain of CtAtg15 (CtAtg15 (73-475, S330A), where the active center serine (S330) was replaced with alanine to inactivate its enzymatic activity for preventing liposome disruption. Using flotation assays to evaluate the binding between the protein and liposomes, I found that CtAtg15 bound most strongly to liposomes at pH 4.0, which correlates with the degradation activity (Fig. 2B). The pH of the vacuolar environment in *S. cerevisiae* ranges from 5.5 to 6.5 (Preston et al., 1989; Plant et al., 1999), while the vacuolar environment of the thermophilic filamentous fungus *C. thermophilum* could differ. The extracellular cellulase produced by *C. thermophilum* exhibits optimal catalytic activity at pH 4.0 (Liu et al., 2005), suggesting that *C. thermophilum* prefers a more acidic environment than *S. cerevisiae*. This preference could explain why CtAtg15 favors a pH of 4.0, which is more acidic than the vacuolar environment of *S. cerevisiae*.

pH-Dependent Conformational Change of CtAtg15

Next, to investigate the molecular mechanism of substrate recognition by CtAtg15, I

measured the circular dichroism (CD) spectra of CtAtg15 (73-475, S330A) at pH 4.0, where membrane binding affinity is high, and at pH 6.8, where it is low, and evaluated the structural changes induced by pH. As a result, notable spectral differences were observed under pH 4.0 and pH 6.8. At pH 4.0, the CD signal around 220 nm was relatively weak, with a negative peak observed near 235 nm (Fig. 3). On the other hand, at pH 6.8, a strong negative peak was observed around 220 nm, which is a spectral feature indicating the presence of a typical α-helix structure (Fig. 3). Additionally, when the CD spectrum was measured after heat denaturation for comparison, the CD signal nearly disappeared, and the features associated with the secondary structure were no longer observed (Fig. 3). This indicates that the secondary structure of the protein was disrupted by heat treatment, leading to complete denaturation. These results of CD analysis suggest that the protein takes a more stable folded structure under neutral conditions, while under acidic conditions, the α-helical structure loosens, potentially becoming more flexible.

Inability of CtAtg15 to Disintegrate Yeast Plasma Membranes

I examined whether recombinant CtAtg15 could disintegrate plasma membranes of budding yeast based on the already established proteinase K protection assay (Watanabe et al., 2023). In this assay, proteins in the solution are degraded by proteinase K, while proteins within vesicles remain protected from proteolytic degradation. In the other hand, if Atg15 disintegrates vesicle membranes, cargo proteins become accessible to proteinase K and are degraded. In this assay, I focused on the degradation of Ape1, a vacuolar aminopeptidase I. prApe1, a substrate of the Cvt pathway, is enclosed within the Cvt vesicle. When the outer membrane of the Cvt vesicle fuses with the vacuole, the inner-membrane vesicle (Cvt body) is released into the vacuole. This means prApe1 is enclosed within Cvt vesicles or Cvt bodies and/or vacuoles (Klionsky et al., 1992; Harding et al., 1996; Shintani et al., 2002). When prApe1 is exposed to solution, it gets cleaved by proteinases to produce dApe1. Therefore, dApe1 can be used to investigate if CtAtg15 disintegrates membranes of the vesicles enclosing prApe1. As a result, consistent with previous research (Watanabe et al., 2023), when using the 15,000 xg membrane fraction obtained from the lysate of *pep4*Δ*atg15*Δ cells as the substrate, prApe1 was resistant to proteinase K treatment at two different temperatures (Fig. 4A). In contrast, prApe1 was degraded by simultaneous treatment with CtAtg15 and proteinase K. However, when using spheroplasts, yeast cells with cell walls digested and plasma membranes exposed, as the substrate, prApe1 was resistant to simultaneous treatment with CtAtg15 and proteinase K (Fig.

4B), but prApe1 was degraded when treated with the detergent Triton X-100 instead of CtAtg15. These results suggests that CtAtg15 can disintegrate both the membranes of vacuols and Cvt bodies, but not plasma membranes of spheroplasts.

Positive Correlation Between CtAtg15 Membrane Binding and Membrane Curvature

I hypothesized that the inability of CtAtg15 to degrade the spheroplast plasma membrane might be primarily influenced by either membrane curvature or the presence of surface glycans. Regarding the former, the spheroplast can be considered as a vesicle with a diameter of 3-5 μm, exhibiting a membrane curvature that is smaller than and closer to zero compared to that of Cvt bodies or vacuolar membranes. In this hypothesis, Atg15 targets only membranes with a certain level of positive curvature. For the latter, I considered that glycans derived from glycoproteins or glycolipids on the plasma membrane might act as a protective barrier against Atg15.

To test these hypotheses, I examined whether recombinant CtAtg15 binds to giant unilamellar vesicles (GUVs). GUVs, composed solely of lipids and with diameters of several micrometers, lack glycan modifications, allowing us to determine whether the substrate recognition of CtAtg15 depends more significantly on membrane curvature or glycan presence. At pH 7.4, mRuby3-CtAtg15 (73-475, S330A) showed minimal binding to the vesicles (with slight fluorescence leakage from NBD-PE observed) (Fig. 5A). In contrast, at pH 4.0, it bound tightly to large unilamellar vesicles (LUVs) with diameters in the hundred-nanometer range, while exhibiting poor binding to GUVs (Fig. 5B). Additionally, I checked that mRuby3-CtAtg15 bound to liposomes similarly to CtAtg15 without mRuby3 tag by flotation assay (data not shown), confirming that the fluorescent protein tag did not affect membrane binding affinity.

Next, I further investigated the correlation between CtAtg15 membrane binding and liposome sizes. Liposomes prepared by the hydration method (the same method used in Fig. 1b) were utilized as the input and sequentially filtered by polycarbonate filters with indicated pores to obtain liposomes of the target sizes. The sizes of the filtered liposomes were measured by dynamic light scattering, confirming that their sizes were effectively adjusted by the filtration process (Fig. 5C). Subsequently, flotation assays using liposomes in the 800 nm to 100 nm range showed that CtAtg15 membrane binding increased as liposome size decreased (Fig. 5D). I also attempted the same experiment with GUVs of several micrometers in diameter. However, during GUV preparation, LUVs were also formed and mixed in, making it challenging to isolate pure GUVs by filtration for flotation assays. In summary, these results

demonstrate that CtAtg15 shows higher binding affinity to smaller liposomes, indicating a positive correlation between membrane curvature and CtAtg15 membrane binding.

Contribution of Basic Amino Acid Residues Around the Active Center to Enzymatic Activity

A previous study (Watanabe et al., 2023) revealed that the lipase domain of CtAtg15 is activated through proteolytic cleavage by a protease at the S159-V160 site. This cleavage induces a conformational change in the protein, exposing the active center S330 to the solvent, thereby facilitating substrate access. Structure prediction using ColabFold (Mirdita et al., 2022) indicates that the region exposed by cleavage is positively charged (Watanabe et al., 2023). I focused on several basic amino acids residues (K112, R223, H225, K240, H329, H439, and K440) located in this positively charged region, which is thought to be important for enzymatic activity (Fig. 6A). To investigate the contribution of these basic amino acids residues to enzymatic activity, I purified recombinant mutant CtAtg15 proteins with each of these basic amino acids residues individually substituted with alanine (K112A, R223A, H225A, K240A, H329A, H439A, and K440A) and examined their affinity for liposomes by flotation assay. As a result, all mutants showed binding affinity to liposomes comparable to that of S330A, indicating that the membrane binding affinity of these mutants were not reduced (Fig. 6B).

Next, I examined the ability of cells expressing these CtAtg15 mutants, which replace endogenous Atg15, to degrade Cvt bodies. I enabled the targeting of the lipase domains of these CtAtg15 mutants to the vacuole by fusing the Pho8TMD (1-26) to their N-terminus. Pho8TMD facilitates the transport of the lipase domain to the vacuole via the Pho8 pathway (Cowles et al., 1997). As a result, all mutants except for K112A showed a reduction or complete absence of the mApe1 band, indicating that degradation of Cvt bodies was halted (Fig. 6C). The loss of activity with the H439A mutation can be explained by the fact that H439 is one of the catalytic triads essential for lipase activity (Watanabe et al., 2023). These results suggest that while these basic amino acids residues do not contribute to the membrane binding affinity of the protein, they play an important role in enzymatic activity.

Discussion

Structural Changes of CtAtg15 After Binding to Membrane

The CD spectra measurements of CtAtg15 (73-475, S330A) at pH 4.0 and neutral conditions (pH 6.8) suggest possible differences in secondary structures under these conditions. However, it is important to note that the CD spectra were measured in buffer without liposomes, meaning the protein was not bound to its substrate. There remains the possibility that Atg15 undergoes structural changes or stabilization upon membrane binding. Therefore, structural analysis of Atg15 in the presence of vesicles or when bound to lipids would likely provide deeper insights into the molecular mechanisms underlying its membrane binding affinity.

Membrane Curvature and Atg15

This study showed a positive correlation between CtAtg15 membrane binding affinity and membrane curvature (Fig. 5). The established membrane curvature-sensing mechanisms of proteins often rely on specific structures, such as the ALPS motif and BAR domains (Bigay et al., 2005; Peter et al., 2004). ALPS motif consists of an amphipathic helix, typically 20 to 40 amino acids residues in length, characterized by hydrophobic and hydrophilic faces. When a membrane has sufficient curvature to expose the hydrophobic region, the hydrophobic face of the ALPS motif inserts into it, while the hydrophilic face interacts with the lipid headgroup regions, enabling selective binding to highly curved membranes. I propose the potential ALPS motif in ScAtg15 and CtAtg15 based on their amino acid residues sequences and predicted protein structures. Both ScAtg15 (304-321) and CtAtg15 (302-319) consist of 18 amino acids residues, and arranging these amino acids residues into an α-helix forms a hydrophobic face on one side and a hydrophilic face on the opposite side (Fig. 7). Protein structure predictions using AlphaFold3 suggest that both motifs actually adopt an amphipathic alpha-helical structure (Fig. 7). Furthermore, aligning ScAtg15 and CtAtg15 shows that these potential ALPS motifs occupy nearly the same spatial position, orienting their faces in the same direction. I therefore consider these amphipathic α-helix could be a potential ALPS motifs.

However, an ALPS motif generally exhibits high affinity for membranes with high curvature, typically around a radius of 25–50 nm. For example, ArfGAP1 shows a significant increase in membrane binding as the liposome diameter decreases from 88 nm to 31 nm (Bigay et al., 2005; Drin et al., 2007) and Vps41 exhibits a similar trend as the diameter decreases from 50 nm to 30 nm (Cabrera et al., 2010), facilitated by their ALPS motifs. Since CtAtg15 could

degrade yeast vacuolar membranes (Fig. 4), which have a diameter of 1–3 μm (Michaillat et al., 2012), it must therefore be able to bind to vesicles of at least this size. Given that ALPS motifs do not typically recognize vesicles with such low curvature, even if Atg15 possesses a functional ALPS motif, an additional mechanism might be required to recognize membranes with lower curvatures.

It has also been reported that intrinsically disordered proteins, which lack specific structures like the BAR domain or ALPS motif, can act as effective sensors for highly curved membranes (Zeno et al., 2019). Disordered proteins are thought to sense curvature through mechanisms involving conformational entropy and net negative charge. When tethered to the membrane surface, disordered proteins experience a decrease in conformational entropy. However, when the membrane is curved, the reduced entropy is restored due to the space created by lipid packing defects, which contributes to the membrane binding affinity. Simultaneously, lipid packing defects often separate disordered proteins, which are typically negatively charged, from the negatively charged head groups of phospholipids, thereby contributing to membrane binding affinity. My CD analysis results suggest that CtAtg15 adopts a more folded structure under neutral pH, but becomes more flexible under acidic conditions (Fig. 3). Since Atg15 exhibits higher activity in acidic environments, it may achieve membrane binding and curvature recognition through increased disorder in these conditions.

Contributions of Basic Amino Acids Residues Around the Active Center in CtAtg15

In this study, I confirmed that the basic amino acids residues near the active center, which form a positively charged region around the active center, do not contribute to membrane binding (Fig. 6B). However, all basic amino acids residues except for K240 contribute to its enzymatic activity (Fig. 6C). CtAtg15 can degrade micelles composed of neutral phospholipids such as PtdCho (Watanabe et al., 2023), suggesting that electrostatic interactions between negatively charged phospholipids, such as PtdSer or PtdIns, and positively charged amino acid residues are not required for its membrane binding. Therefore, this positively charged region may play an important role in its enzymatic activity, independent of interactions with the negatively charged head groups of phospholipids. Possible roles of this region include assisting in substrate positioning, stabilizing the environment around the catalytic center, or facilitating proton transfer and charge stabilization during catalysis.

Effects of Glycans on Atg15 Activity

In this study, I focused on the influence of membrane curvature, but glycans may also play a role in protecting membranes from enzymatic degradation. In mammalian cells, there are more than 100 lysosomal membrane proteins, many of them are highly glycosylated toward the lumenal side (Fukuda, 1990). Glycosylations are considered important for protecting the protein itself from degradation by lysosomal proteinase, and it is also suggested that they protect the lysosomal membranes as well (Schwake et al., 2013; Xiong and Zhu, 2016; Li and Pfeffer, 2016). Therefore, it is likely that a similar mechanism occurs in the vacuoles of yeast cells.

Other Possible Hypotheses

Furthermore, it has been hypothesized that the vacuolar membrane possesses a mechanism to rapidly repair damage caused by Atg15. However, in the study by Kagohashi et al., it was observed that Atg15 was bound to the membranes of ABs but not localized near the vacuolar membrane. This suggests that Atg15 does not initially bind to the vacuolar membrane.

Future Perspectives

Due to technical limitations, I have only been able to observe the membrane binding affinity of Atg15 to membranes with positive curvature. Therefore, future studies should focus on understanding how Atg15 interacts with membranes that have negative curvature. To investigate this, it will be necessary to encapsulate Atg15 within liposomes. Research on liposomes encapsulating various substances has been actively conducted, particularly in drug delivery systems (DDS). Methods like microfluidics (Tan et al., 2006; Stachowiak et al., 2008) or cell-penetrating peptides (Miwa and Kamiya, 2022) are effective for incorporating purified proteins into liposomes without causing denaturation. I plan to use these techniques in future studies to explore how Atg15 inside a vesicle interacts with membranes exhibiting negative curvature.

Additionally, the role of glycans needs to be explored. The density of glycans on cell membranes varies widely depending on factors such as cell type, membrane region, and cell conditions, which makes it challenging to generalize. Therefore, as a future research direction, I aim to investigate how increasing glycans on liposome membranes affect membrane binding affinity of Atg15, with the goal of relating these findings to *in vivo* membrane environments. Since disruption of the vacuolar membrane causes cell death (Stolp et al., 2022), it is likely that its protection is ensured by multiple mechanisms, such as a combination of curvature selectivity and glycan barriers.

Materials and Methods

Strains, Media and Growth Conditions

SHuffle T7 Express Competent *E. coli* cells (New England Biolabs) were used for expression of recombinant proteins. The yeast strains used in this study are listed in Table 1. The *YPT7*, *ATG15* and *PEP4* genes were disrupted by DNA fragments amplified by polymerase chain reaction (PCR) from plasmids pFA6a-hphNT1 and pFA6a-kanMX6, respectively (Longtine et al., 1998; Janke et al., 2004). Primers used for gene disruptions are listed in Table 2. Yeast cells were cultured in SDCA medium (0.17% Difco yeast nitrogen base without amino acids and ammonium sulfate, 0.5% ammonium sulfate, 0.5% Bacto casamino acids, 2% glucose) with appropriate supplements.

Plasmids

The plasmids used in this study are listed in Table 3. The pETDuet-1 vectors were used for the *E. coli* expression. To construct the expression plasmid for mRuby3-CtAtg15(73–475, S330A), DNA fragments for mRuby3 and CtAtg15 were amplified by PCR and assembled into the vector using the NEBuilder HiFi DNA Assembly. The N-terminal mRuby3 and C-terminal CtAtg15 were directly fused without any restriction enzyme site or a linker between them. To construct the expression plasmids for mutant CtAtg15, DNA fragments were amplified by inverse PCR with primers containing the mutation, using pETDuet-1[CtAtg15(73–475, S330A)] as the template. A 6xHis tag was fused to the N-terminus of the recombinant protein genes. The *S. cerevisiae* expression plasmids were based on pRS313 vector. DNA fragments for Pho8TMD (1-26) and the lipase domain of CtAtg15 (73-475) were amplified by PCR and inserted into the vector, with Pho8TMD at the N-terminus and CtAtg15 at the C-terminus, with an *Nhe*I site inserted between them. Amplification of plasmids was carried out using *E. coli* cells (DH5α) grown in LB medium (1% Bacto tryptone, 0.5% Bacto yeast extract, 1% NaCl) with 100 μg/mL ampicillin.

Purification of Recombinant Proteins

Target proteins with His-tag were expressed in *E. coli* SHuffle T7 cells cultured in LB medium supplemented with 100 μg/mL ampicillin at 37°C. When the optical density of the culture at 600 nm reached ~0.8, IPTG (9030, TaKaRa) was added to a final concentration of

0.3 mM, and cultured at 16°C for 20 h to induce protein expression. After induction of protein expression, the cells were harvested, resuspended in lysis buffer (50 mM Tris-HCl [pH 8.0], 500 mM NaCl, and 20 mM imidazole), disrupted by sonication and centrifuged to pellet the insoluble debris. Cleared lysates were filtered through a 0.22-μm filter, and proteins were purified using TALON® Metal Affinity Resin (635502, TaKaRa) according to the manufacturer's instructions. Proteins were further purified by size exclusion chromatography using a Superdex 200 10/300 increase column (Cytiva), with an elution buffer of 20 mM Tris-HCl (pH 8.0) and 150 mM NaCl.

Liposome Preparation

The following lipids were purchased from the manufacturers as noted: 18:1-12:0 NBD-PE (1-oleoyl-2-{12-[(7-nitro-2-1,3-benzoxadiazol-4-yl)amino]dodecanoyl}-sn-glycero-3-phosphoethanolamine) (810156C, Avanti Polar Lipids, Inc.), DOPC (1,2-dioleoyl-sn-glycero-3-phosphocholine) (850375C, Avanti Polar Lipids, Inc.), DOPE (1,2-dioleoyl-sn-glycero-3-phosphoethanolamine) (850725C, Avanti Polar Lipids, Inc.) and DOPS (1,2-dioleoyl-sn-glycero-3-phospho-L-serine) (840035P, Avanti Polar Lipids, Inc.). The lipid mixtures were dried under nitrogen gas and hydrated in 50 mM acetate buffer (pH 3.1, 4.0, and 5.0) or 50 mM MES buffer (pH 6.0)/150 mM NaCl/0.5 mM EDTA for 30 min at 50°C and vortexed for 1 min. If necessary, the liposome suspension was extruded sequentially through polycarbonate filters with pore sizes of 800, 400, 200, 100 nm using a hand extruder (Avanti Polar Lipids, Inc.).

Thin-Layer Chromatography (TLC)

NBD-PE–containing liposomes (80 μM; DOPC/DOPE/18:1-12:0 NBD-PE = 50/40/10) were incubated with 20 μM purified CtAtg15(73–475) and 4.5 μM proteinase K in 50 μL assay buffer for the indicated time periods at 30°C. To measure the activities of CtAtg15(73–475) at various pH conditions, the reactions were carried out in different buffers as follows: 50 mM acetate buffer (pH 3.1, 4.0, and 5.0) and 50 mM MES buffer (pH 6.0). These buffers were supplemented with 150 mM NaCl and 0.5 mM EDTA. After incubation, lipid extraction was performed using the Bligh and Dyer method (Bligh and Dyer, 1959) with modifications. Briefly, 750 μL of 2:1 chloroform/methanol was added to the samples and vortexed for 10 min to extract lipids. One hundred μl of water was added to the samples, which were then vortexed for 10 min. The organic phase was separated by centrifugation at 1,000*g* for

2 min, collected, and dried under nitrogen gas. The resulting lipid film was dissolved in chloroform and analyzed by TLC using chloroform/ethanol/water (65:25:4) as a developing solvent. NBD signals were detected and quantified using a ChemiDoc imaging system with ImageLab software (Bio-Rad). TLC plates were purchased from Merck Millipore.

Liposome Flotation Assay

To remove aggregated proteins, purified proteins were subjected to centrifugation at 10,000*g* for 10 min at 4°C. 5 μM of proteins was mixed with 2 mM of liposomes in 100 μl assay buffer at 25°C for 10 min. 200 μl of a 60% sucrose in assay buffer was added to adjust the sucrose concentration to 40%. The suspension was layered with three cushions: 550 μl of 30% sucrose, 550 μl of 10% sucrose, and 200 μl of 0% sucrose solution. It was then ultracentrifuged at 170,000*g* for 90 min at 25°C. After centrifugation, four 400 μl fractions were sequentially collected from the top to the bottom, and the proteins precipitated by TCA were analyzed by SDS-PAGE. The gels were visualized with IR-LAS 1000 imaging system (FUJIFILM). The buffers used were as follows: 50 mM acetate buffer (pH 3.1, 4.0, and 5.0) and 50 mM MES buffer (pH 6.0), each supplemented with 150 mM NaCl and 0.5 mM EDTA.

CD Spectroscopy

The structure of each protein in solution (0.1 mg/ml) was determined using a standardized methodology in a 1.0 cm path length quartz cuvette with a Jasco J-725 CD spectropolarimeter. Briefly, each CD spectrum, recording both ellipticity and absorbance values, was obtained over a wavelength range of 200 to 300 nm, with a scan rate of 100 nm/min and a response time of 1.0 sec. Each spectrum represented the result of a single scan. Temperature was maintained at 25°C using the instrument's integrated cooling system. Thermal-induced denaturation of the protein was performed at 60°C for 20 min. The protein spectrum was measured in either a 50 mM acetate buffer (pH 4.0) or a 10 mM Tris-HCl buffer (pH 6.8), both containing 100 mM NaCl.

Proteinase K Protection Assay

Yeast cells were grown to log phase, collected, converted to spheroplasts and mechanically disrupted with 3.0-μm polycarbonate filters (Whatman) in lysis buffer (HES1.0 buffer: 20 mM HEPES [pH 7.5], 5 mM EDTA, and 1 M sorbitol). After cell debris was removed by centrifugation, cell lysates were centrifuged at 15,000*g* for 15 min. The pellets were

resuspended in $AES_{1.0}$ buffer (80 mM potassium acetate [pH 5.0], 5 mM EDTA and 1 M sorbitol), divided into aliquots and treated with or without 20 μM CtAtg15(73–475), 1% Triton X-100, and 4.5 μM proteinase K (9034, Takara Bio) in 50 μl buffer. The reactions were terminated by addition of 15% TCA Precipitants were washed with acetone and dissolved in SDS-PAGE sample buffer containing 4 mM Pefabloc SC (11429876001, Roche). Equivalent protein amounts were subjected to immunoblotting analysis.

Immunoblotting Analysis

Cell lysates were prepared by the alkaline lysis method (Horvath and Riezman, 1994) and subjected to SDS–PAGE. SDS-PAGE was performed using a 10% polyacrylamide gel. Proteins were transferred polyvinylidene fluoride (PVDF) membranes (Immobilon-P, Millipore) utilizing a semi-dry transfer apparatus (Bio-Rad) at 2 mA per 1 cm^2 for 45 min. Following transfer, the membranes were blocked with 4% skim milk in Tris-buffered saline containing 0.05% tween 20 (TBST) for 30 min at room temperature (RT). Membranes were then incubated with mouse monoclonal anti-GFP antibody B-2 (1:5000) (Santa Cruz Biotechnology), anti-Ape1 (1:5000) (Suzuki et al., 2002) antiserum for 90 min at RT. Subsequently, membranes were washed 3 times with TBST and treated with Horseradish peroxidase (HRP)-labeled anti rabbit or mouse secondary antibodies (Promega) at a dilution of 1:5000 for 45 min following a further washing cycle with TBST. Chemiluminescent signals generated by the enhanced chemiluminescence (ECL) reagent (GE Healthcare) were detected with IR-LAS 1000 imaging system (FUJIFILM).

GUV Preparation

The protocol for the GUV preparation was basically based on that described previously (Horger et al., 2009). Briefly, 1% low-melting-point agarose gel, dissolved by boiling, was thinly spread over a cover glass and left it at 40°C for 3 hours to dry the agarose gel. A total of 310 nmol of lipids were dried under nitrogen gas to eliminate the solvent and then redissolved in 50 μl of chloroform. The redissolved lipid were put on a hydrated film of agarose, spread thinly, and nitrogen gas was blown over them to form a lipid film on the agarose gel. An ionic solution, used for an experiment, was placed on the hybrid films of agarose and lipids, and incubated at 37°C for 2 hours to obtain GUVs. To the 50 μl GUV solution, 0.5 μg of protein was added, incubated at 25°C for 10 min, and then imaging was performed.

References

BLIGH EG, DYER WJ. (1959). A rapid method of total lipid extraction and purification. Can J Biochem Physiol. 37(8):911-7.

Bigay J, Casella JF, Drin G, Mesmin B, Antonny B. (2005). ArfGAP1 responds to membrane curvature through the folding of a lipid packing sensor motif. EMBO J. 24(13):2244-53.

Boutouja F, Stiehm CM, Mastalski T, Brinkmeier R, Reidick C, El Magraoui F, Platta HW. (2019). Vps10-mediated targeting of Pep4 determines the activity of the vacuole in a substrate-dependent manner. Sci Rep. 9(1):10557.

Brachmann CB, Davies A, Cost GJ, Caputo E, Li J, Hieter P, Boeke JD. (1998). Designer deletion strains derived from *Saccharomyces cerevisiae* S288C: a useful set of strains and plasmids for PCR-mediated gene disruption and other applications. Yeast. 14(2):115-32.

Cabrera M, Langemeyer L, Mari M, Rethmeier R, Orban I, Perz A, Bröcker C, Griffith J, Klose D, Steinhoff HJ, Reggiori F, Engelbrecht-Vandré S, Ungermann C. (2010). Phosphorylation of a membrane curvature-sensing motif switches function of the HOPS subunit Vps41 in membrane tethering. J Cell Biol. 191(4):845-59.

Cowles CR, Snyder WB, Burd CG, Emr SD. (1997). Novel Golgi to vacuole delivery pathway in yeast: identification of a sorting determinant and required transport component. EMBO J. 16(10):2769-82.

Drin G, Casella JF, Gautier R, Boehmer T, Schwartz TU, Antonny B. (2007). A general amphipathic alpha-helical motif for sensing membrane curvature. Nat Struct Mol Biol. 14(2):138-46.

Epple UD, Suriapranata I, Eskelinen EL, Thumm M. (2001). Aut5/Cvt17p, a putative lipase essential for disintegration of autophagic bodies inside the vacuole. J Bacteriol. 183(20):5942-55.

Fukuda M. (1990). Lysosomal membrane glycoproteins; structure, biosynthesis, and trafficking to lysosome. Seikagaku. 62(10):1225-40.

Harding TM, Hefner-Gravink A, Thumm M, Klionsky DJ. (1996). Genetic and phenotypic overlap between autophagy and the cytoplasm to vacuole protein targeting pathway. J Biol

Chem. 271(30):17621-4.

Horger KS, Estes DJ, Capone R, Mayer M. (2009). Films of agarose enable rapid formation of giant liposomes in solutions of physiologic ionic strength. J Am Chem Soc. 131(5):1810-9.

Horvath A, Riezman H. (1994). Rapid protein extraction from *Saccharomyces cerevisiae*. Yeast. 10(10):1305-10.

Hirata E, Shirai K, Kawaoka T, Sato K, Kodama F, Suzuki K. (2021). Atg15 in *Saccharomyces cerevisiae* consists of two functionally distinct domains. Mol Biol Cell. 32(8):645-663.

Janke C, Magiera MM, Rathfelder N, Taxis C, Reber S, Maekawa H, Moreno-Borchart A, Doenges G, Schwob E, Schiebel E, Knop M. (2004). A versatile toolbox for PCR-based tagging of yeast genes: new fluorescent proteins, more markers and promoter substitution cassettes. Yeast. 21(11):947-62.

Kagohashi Y, Sasaki M, May AI, Kawamata T, Ohsumi Y. (2023). The mechanism of Atg15-mediated membrane disruption in autophagy. J Cell Biol. 222(12):e202306120.

Klionsky DJ, Cueva R, Yaver DS. (1992). Aminopeptidase I of *Saccharomyces cerevisiae* is localized to the vacuole independent of the secretory pathway. J Cell Biol. 119(2):287-99.

Li J, Pfeffer SR. (2016). Lysosomal membrane glycoproteins bind cholesterol and contribute to lysosomal cholesterol export. Elife. 5:e21635.

Liu SA, Li DC, E SJ, Zhang Y. (2005). Cloning and expressing of cellulase gene (cbh2) from thermophilic fungi Chaetomium thermophilum CT2. Sheng Wu Gong Cheng Xue Bao. 21(6):892-9.

Longtine MS, McKenzie A 3rd, Demarini DJ, Shah NG, Wach A, Brachat A, Philippsen P, Pringle JR. (1998). Additional modules for versatile and economical PCR-based gene deletion and modification in *Saccharomyces cerevisiae*. Yeast. 14(10):953-61.

Michaillat L, Baars TL, Mayer A. (2012). Cell-free reconstitution of vacuole membrane fragmentation reveals regulation of vacuole size and number by TORC1. Mol Biol Cell. 23(5):881-95.

Millen JI, Krick R, Prick T, Thumm M, Goldfarb DS. (2009). Measuring piecemeal microautophagy of the nucleus in *Saccharomyces cerevisiae*. Autophagy. 5(1):75-81.

Mirdita M, Schütze K, Moriwaki Y, Heo L, Ovchinnikov S, Steinegger M. (2022). ColabFold: making protein folding accessible to all. Nat Methods. 19(6):679-682.

Miwa A, Kamiya K. (2022). Control of Enzyme Reaction Initiation inside Giant Unilamellar Vesicles by the Cell-Penetrating Peptide-Mediated Translocation of Cargo Proteins. ACS Synth Biol. 11(11):3836-3846

Mizushima N, Yoshimori T, Ohsumi Y. (2011). The role of Atg proteins in autophagosome formation. Annu Rev Cell Dev Biol. 27:107-32.

Peter BJ, Kent HM, Mills IG, Vallis Y, Butler PJ, Evans PR, McMahon HT. (2004). BAR domains as sensors of membrane curvature: the amphiphysin BAR structure. Science. 303(5657):495-9.

Plant PJ, Manolson MF, Grinstein S, Demaurex N. (1999). Alternative mechanisms of vacuolar acidification in H(+)-ATPase-deficient yeast. J Biol Chem. 274:37270-9.

Preston RA, Murphy RF, Jones EW. (1989). Assay of vacuolar pH in yeast and identification of acidification-defective mutants. Proc Natl Acad Sci U S A. 86:7027-31.

Schwake M, Schröder B, Saftig P. (2013). Lysosomal membrane proteins and their central role in physiology. Traffic. 14(7):739-48.

Shintani T, Huang WP, Stromhaug PE, Klionsky DJ. (2002). Mechanism of cargo selection in the cytoplasm to vacuole targeting pathway. Dev Cell. 3(6):825-37.

Stachowiak JC, Richmond DL, Li TH, Liu AP, Parekh SH, Fletcher DA. (2008). Unilamellar vesicle formation and encapsulation by microfluidic jetting. Proc Natl Acad Sci U S A. 105(12):4697-702.

Stolp ZD, Kulkarni M, Liu Y, Zhu C, Jalisi A, Lin S, Casadevall A, Cunningham KW, Pineda FJ, Teng X, Hardwick JM. (2022). Yeast cell death pathway requiring AP-3 vesicle trafficking leads to vacuole/lysosome membrane permeabilization. Cell Rep. 39(2):110647.

Suzuki K, Kamada Y, Ohsumi Y. (2002). Studies of cargo delivery to the vacuole mediated by autophagosomes in *Saccharomyces cerevisiae*. Dev Cell. 3(6):815-24.

Takeshige K, Baba M, Tsuboi S, Noda T, Ohsumi Y. (1992). Autophagy in yeast demonstrated

with proteinase-deficient mutants and conditions for its induction. J Cell Biol. 119(2):301-11.

Tan YC, Hettiarachchi K, Siu M, Pan YR, Lee AP. (2006). Controlled microfluidic encapsulation of cells, proteins, and microbeads in lipid vesicles. J Am Chem Soc. 3;128(17):5656-8.

Teter SA, Eggerton KP, Scott SV, Kim J, Fischer AM, Klionsky DJ. (2001). Degradation of lipid vesicles in the yeast vacuole requires function of Cvt17, a putative lipase. J Biol Chem. 276(3):2083-7.

van Zutphen T, Todde V, de Boer R, Kreim M, Hofbauer HF, Wolinski H, Veenhuis M, van der Klei IJ, Kohlwein SD. (2014). Lipid droplet autophagy in the yeast *Saccharomyces cerevisiae*. Mol Biol Cell. 25(2):290-301.

Watanabe Y, Iwasaki Y, Sasaki K, Motono C, Imai K, Suzuki K. (2023). Atg15 is a vacuolar phospholipase that disintegrates organelle membranes. Cell Rep. 42(12):113567.

Xiong J, Zhu MX. (2016). Regulation of lysosomal ion homeostasis by channels and transporters. Sci China Life Sci. 59(8):777-91.

Zeno WF, Thatte AS, Wang L, Snead WT, Lafer EM, Stachowiak JC. (2019). Molecular Mechanisms of Membrane Curvature Sensing by a Disordered Protein. J Am Chem Soc. 41(26):10361-10371.

Tables

Table 1. Yeast strains used in this study

Strain and Genotype	Source
BY4741- *MAT***a** *leu2Δ*0 *ura3Δ*0 *his3Δ*1 *met15Δ*0	Brachmann et al., 1998
Y575- BY4741; *ypt7Δ*::*kanMX*	EUROSCARF
Y5789- BY4741; *atg15Δ*::*kanMX*	EUROSCARF
Y2098- BY4741; *pep4Δ*::*kanMX*	EUROSCARF
GYS1575- *MAT***a** *leu2Δ*0 *ura3Δ*0 *his3Δ*1 *met15Δ*0 *atg15Δ*::*kanMX pep4Δ*::*hphNT1*	Watanabe et al., 2023

Table 2. Primers used in this study

Name	Sequence
pETDuet-1_InversePCR_F	GTCTGGTAAAGAAACCGCTGCTGCGA
pETDuet-1_InversePCR_R	TGGCTGTGGTGATGATGGTGATGGC
CtAtg15(pETDuet-1)_F	TCATCACCACAGCCAGGATCCGGCGCCTGCGGAACACGTCTTTACCCT
CtAtg15(pETDuet-1) _R	GTTTCTTTACCAGACTCGAGTTAACTTTCGTACATCTTCCATGATCC
mRuby3_F	CACCATCATCACCACAGCCAGGATCCGATGGTGTCTAAGGGCGAAGAGCTG
mRuby3_R	CTTGTACAGCTCGTCCATGCCAC
pRS313_InversePCR_F	CTCGAGGGGGGGCCCGGTACCCAGC
pRS313_InversePCR_R	GAGCTCCAATTCGCCCTATAGTGAGT
CYC1_promoter_F	CTCACTATAGGGCGAATTGGAGCTCCATTTGGCGAGCGTTGGTTGGT
CYC1_promoter_R	AGTTCTAGAGCGGCCGCTTAGTGTGTGTATTTGTGTTTGCGTGTCTATAGA
CYC1_terminator_F	TCGATACCGTCGACCTCGAGTCATGTAATTAGTTATGTCACGCTTACA
CYC1_terminator_R	GCTGGGTACCGGGCCCCCCCTCGAGGGCCGCAAATTAAAGCCTTCGAGC
Pho8_TMD_F	TAGAACTAGTGGATCCATGATAATAGTATCCACTGTGGTCTGTATTGGTTTGTTG
Pho8_TMD_R	GCTAGCTAATGCAAAACTGCTTGGAAATGCCAGT
CtAtg15(pRS313)_F	ACGTCAAAGGGCGAAAAACCGTCTAT
CtAtg15(pRS313)_R	GGGATTGTGGATCATGGAAGATGTACGAAAGTTAAGAATTCGATATCAAGC
CtAtg15(S330A)_Inverse_F	CATGCACTGGGTGGTGCTGTGTCGT
CtAtg15(S330A)_Inverse_R	ACAGCACCACCCAGTGCATGGCC
CtAtg15(K112A)_Inverse_F	ACGTTGTGGCTGGCAGCGGAAGA
CtAtg15(K112A)_Inverse_R	TGCCAGCCACAACGTCTGGGCATAC
CtAtg15(R223A)_Inverse_F	TCCGATGGCCTTGCAGGCCATGTATTC
CtAtg15(R223A)_Inverse_R	TGCAAGGCCATCGGATTGCCACCC
CtAtg15(H225A)_Inverse_F	GGCCTTCGCGGCGCAGTATTCG
CtAtg15(H225A)_Inverse_R	TGCGCCGCGAAGGCCATCGG
CtAtg15(K240A)_Inverse_F	GTGATTGGTCTGGCAGGCACCAGTTTAGC
CtAtg15(K240A)_Inverse_R	TGCCAGACCAATCACAATGGTGGAGTTTGTCT
CtAtg15(H329A)_Inverse_F	TGGATTACCGGCGCAGCACTGGG
CtAtg15(H329A)_Inverse_R	TGCGCCGGTAATCCACACATTGCTATTCG
CtAtg15(H439A)_Inverse_F	GGCATTGGGACGGCAAAAATCCGTGC
CtAtg15(H439A)_Inverse_R	TGCCGTCCCAATGCCTACACGCC
CtAtg15(K440A)_Inverse_F	ATTGGGACGCACGCAATCCGTGC
CtAtg15(K440A)_Inverse_R	TGCGTGCGTCCCAATGCCTACACG

Table 3. Plasmids used in this study

Name	Properties	Source
pETDuet-1[CtAtg15$^{73\text{-}475}$]	Plasmid for recombinant CtAtg15$^{73\text{-}475}$	Watanabe et al, 2023
pETDuet-1[CtAtg15$^{73\text{-}475, S330A}$]	Plasmid for recombinant CtAtg15$^{73\text{-}475, S330A}$	Watanabe et al, 2023
pETDuet-1[CtAtg15$^{73\text{-}475, S330A, K112A}$]	Plasmid for recombinant CtAtg15$^{73\text{-}475, S330A, K112A}$	This study
pETDuet-1[CtAtg15$^{73\text{-}475, S330A, R223A}$]	Plasmid for recombinant CtAtg15$^{73\text{-}475, S330A, R223A}$	This study
pETDuet-1[CtAtg15$^{73\text{-}475, S330A, H225A}$]	Plasmid for recombinant CtAtg15$^{73\text{-}475, S330A, H225A}$	This study
pETDuet-1[CtAtg15$^{73\text{-}475, S330A, K240A}$]	Plasmid for recombinant CtAtg15$^{73\text{-}475, S330A, K240A}$	This study
pETDuet-1[CtAtg15$^{73\text{-}475, S330A, H329A}$]	Plasmid for recombinant CtAtg15$^{73\text{-}475, S330A, H329A}$	This study
pETDuet-1[CtAtg15$^{73\text{-}475, S330A, H439A}$]	Plasmid for recombinant CtAtg15$^{73\text{-}475, S330A, H439A}$	This study
pETDuet-1[CtAtg15$^{73\text{-}475, S330A, K440A}$]	Plasmid for recombinant CtAtg15$^{73\text{-}475, S330A, K440A}$	This study
pETDuet-1[mRuby3-CtAtg15$^{73\text{-}475, S330A}$]	Plasmid for recombinant mRuby3-CtAtg15$^{73\text{-}475, S330A}$	This study
pRS313[ScAtg15]	Plasmid for expression of ScAtg15	This study
pRS313[Pho8TMD-CtAtg15$^{73\text{-}475}$]	Plasmid for expression of CtAtg15$^{73\text{-}475}$	This study
pRS313[Pho8TMD-CtAtg15$^{73\text{-}475, S330A}$]	Plasmid for expression of CtAtg15$^{73\text{-}475, S330A}$	This study
pRS313[Pho8TMD-CtAtg15$^{73\text{-}475, K112A}$]	Plasmid for expression of CtAtg15$^{73\text{-}475, K112A}$	This study
pRS313[Pho8TMD-CtAtg15$^{73\text{-}475, R223A}$]	Plasmid for expression of CtAtg15$^{73\text{-}475, R223A}$	This study
pRS313[Pho8TMD-CtAtg15$^{73\text{-}475, H225A}$]	Plasmid for expression of CtAtg15$^{73\text{-}475, H225A}$	This study
pRS313[Pho8TMD-CtAtg15$^{73\text{-}475, K240A}$]	Plasmid for expression of CtAtg15$^{73\text{-}475, K240A}$	This study
pRS313[Pho8TMD-CtAtg15$^{73\text{-}475, H329A}$]	Plasmid for expression of CtAtg15$^{73\text{-}475, H329A}$	This study
pRS313[Pho8TMD-CtAtg15$^{73\text{-}475, H439A}$]	Plasmid for expression of CtAtg15$^{73\text{-}475, H439A}$	This study
pRS313[Pho8TMD-CtAtg15$^{73\text{-}475, K440A}$]	Plasmid for expression of CtAtg15$^{73\text{-}475, K440A}$	This study

Figures

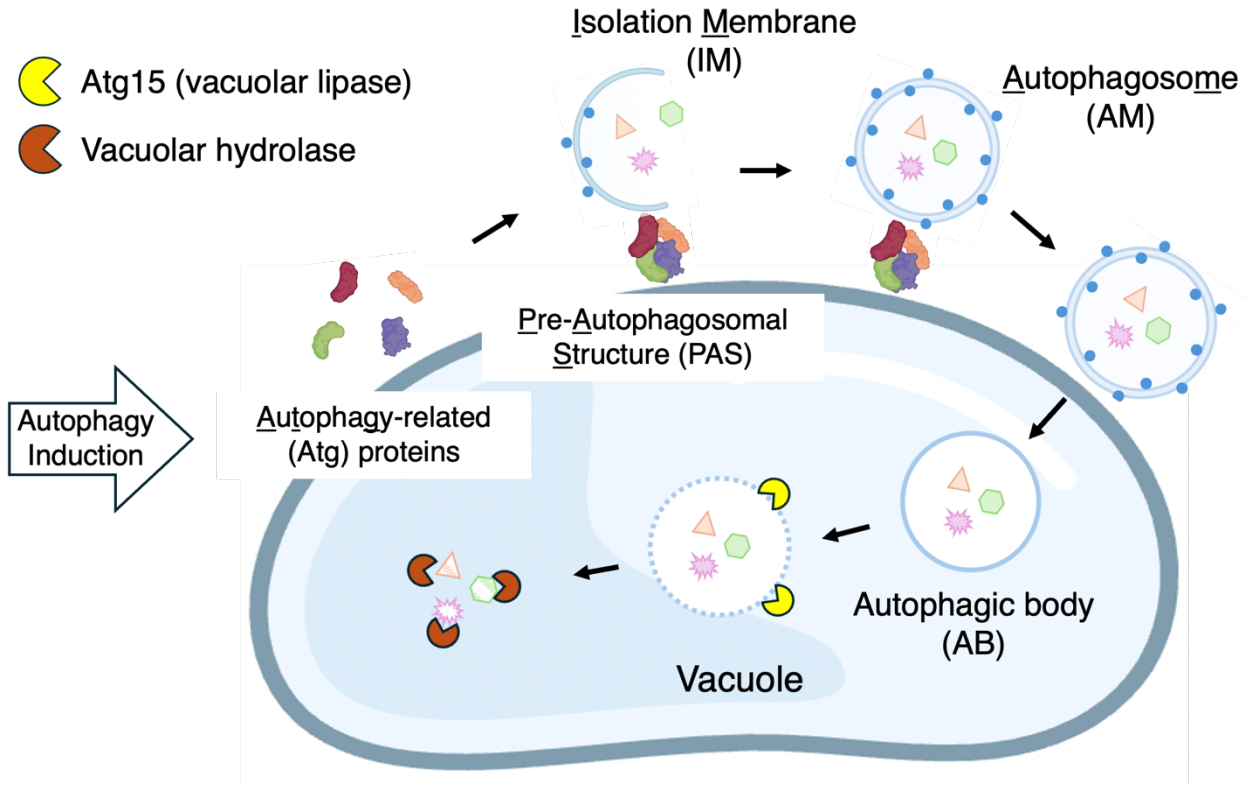

Fig. 1 Autophagy process in yeast

In *S. cerevisiae*, when autophagy is induced, Atg proteins gather near the vacuole membrane, forming the pre-autophagosomal structure (PAS) through liquid-liquid phase separation. Further downstream Atg proteins then assemble, leading to the formation of an isolation membrane (IM) that encapsulates cytoplasmic materials, eventually closing to form a double-membrane autophagosome (AM). The outer membrane fuses with the vacuole, releasing the inner membrane as an autophagic body (AB). Here, the vacuolar phospholipase Atg15 is essential for degrading the AB membrane within the vacuole, allowing vacuolar hydrolases to break down its contents and complete the autophagy process.

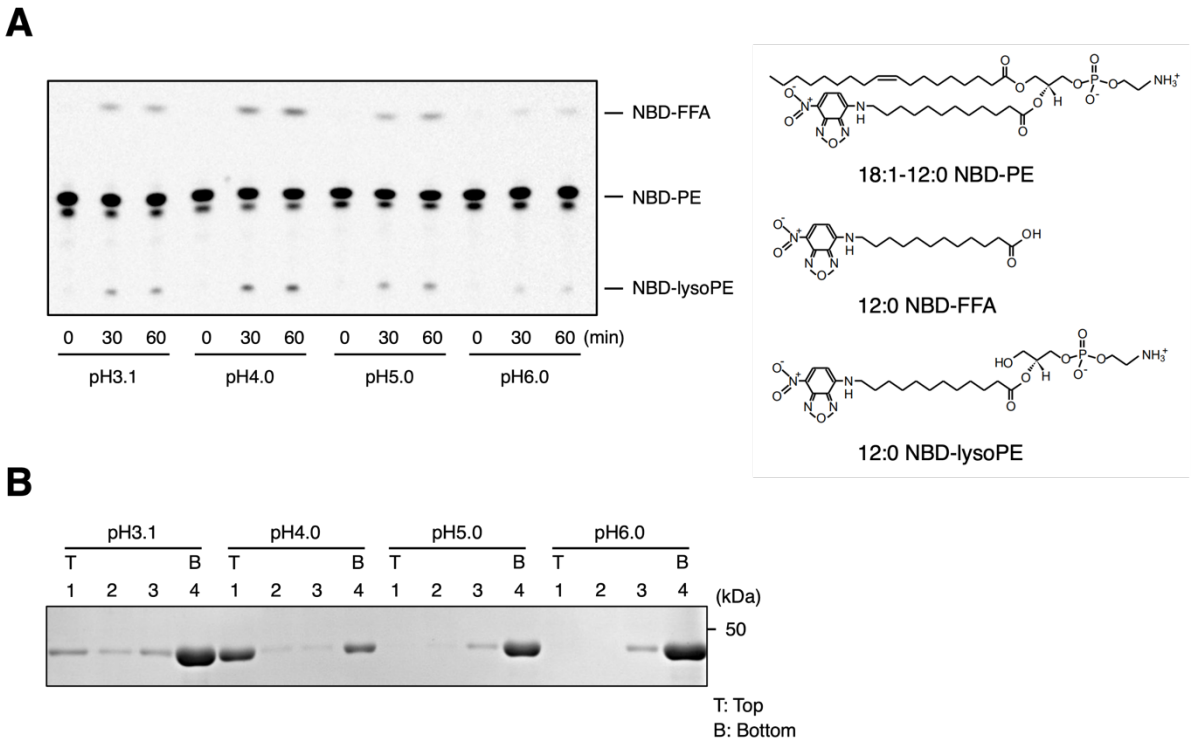

Fig. 2 The ativity of CtAtg15 at different pH

(A) Liposomes (DOPC/DOPE/18:1-12:0 NBD-PE = 50/40/10) and purified CtAtg15 (73-475) were incubated at 30°C for the indicated times at the indicated pH. Phospholipids were extracted and analyzed by thin-layer chromatography (TLC). Chemical structures of 18:1-12:0 NBD-PE, 12:0 NBD-FFA, and 12:0 NBD-lysoPE on the right. (B) Flotation assay. Purified CtAtg15 (73-475, S330A) was incubated with liposomes at indicated pH. After centrifugation, four fractions from the top (T) to bottom (B) were collected and analyzed by SDS-PAGE. Proteins were stained with Coomassie Brilliant Blue.

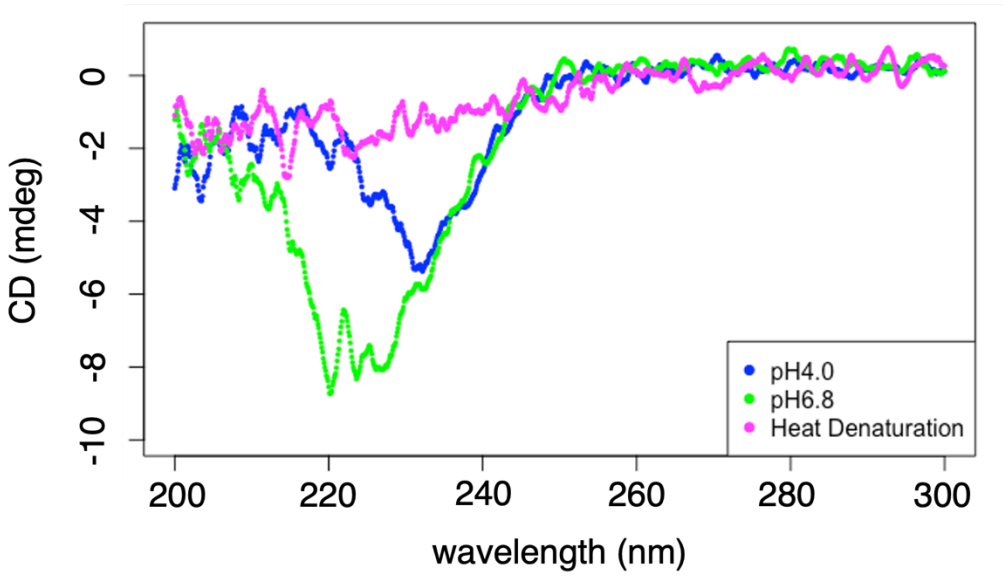

Fig. 3 Circular dichroism (CD) analysis of CtAtg15 at different pH

CD spectra of intact CtAtg15 (73–475, S330A) at 25°C measured in a buffer of indicated pH.

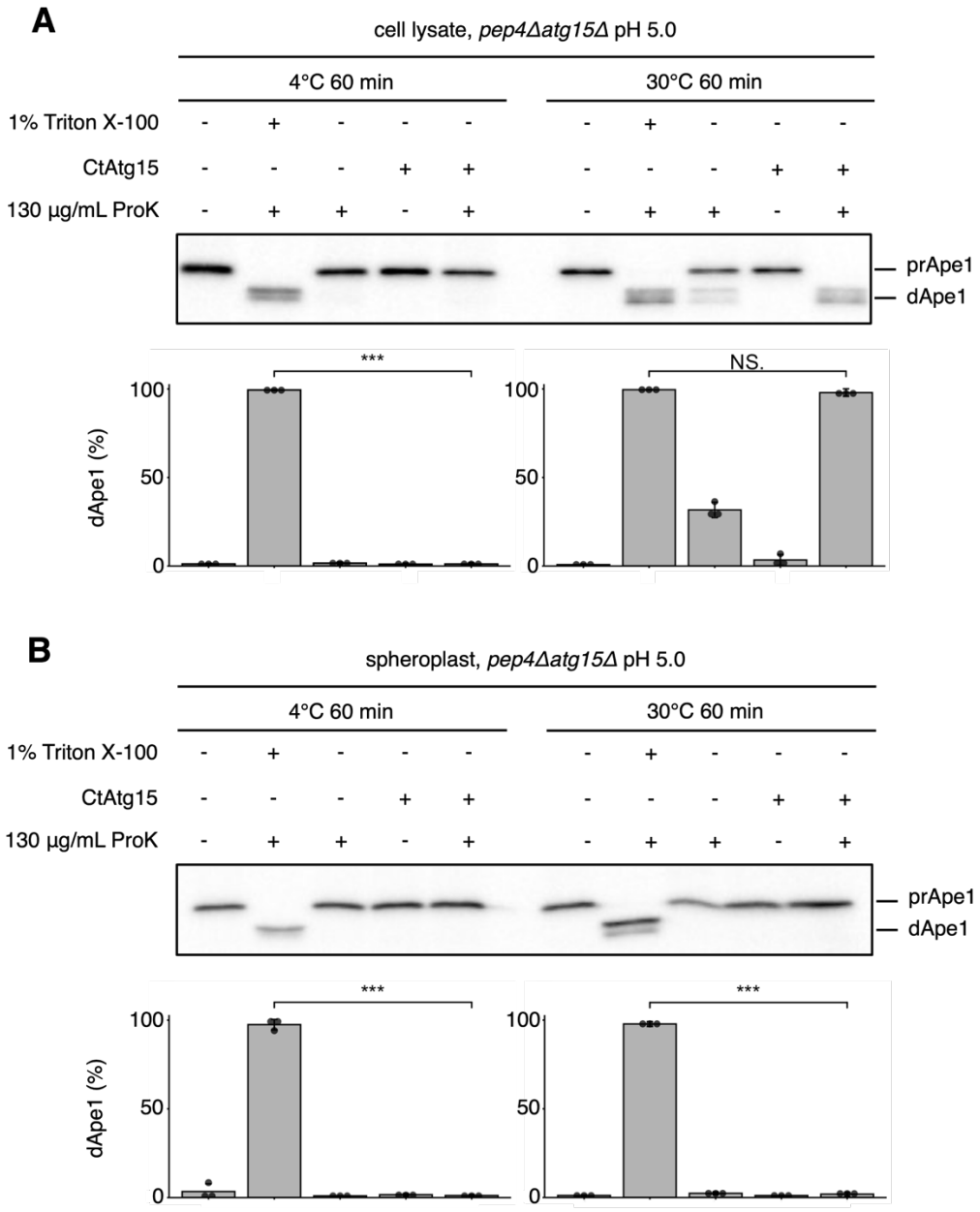

Fig. 4 CtAtg15 does not disintegrate plasma membranes of *S. cerevisiae*

Protease K protection assay. (A) *pep4Δatg15Δ* (GYS1575) cells were grown in YEPD medium, collected, and mechanically disrupted to obtain samples. (B) Cells were processed into spheroplasts to obtain samples. Samples were subjected to immunoblot analysis using anti-Ape1 antisera. prApe1 and dApe1 indicate precursor Ape1 and degraded Ape1, respectively. Error bars indicate standard deviations. Statistical significance was determined using R (ver. 4.2.3) with two-tailed Student's t-test. Data shown are representative of three independent experiments. N.S. indicates not significant. *P < 0.05, **P < 0.01, ***P < 0.001

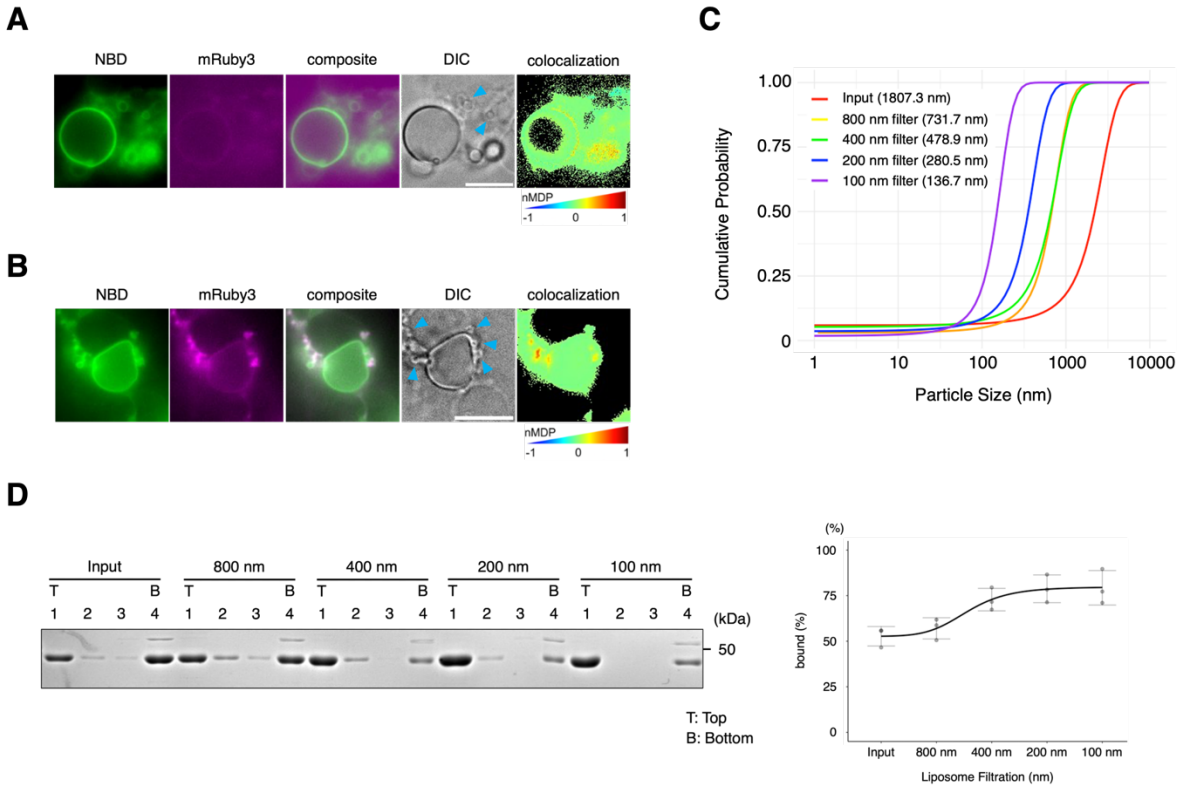

Fig. 5 Positive correlation between CtAtg15 membrane binding and membrane curvature

(A) GUVs were incubated with 0.6 μM mRuby3-CtAtg15 (73-475, S330A) at 25°C in pH6.8 buffer. Fluorescence images of NBD (green) and mRuby3 (magenta) are shown alongside their composite and DIC images. The blue arrowheads indicate LUV. Scale bar: 4 μm. The rightmost panels display pseudo-color colocalization maps generated using the "Colocalization Colormap" plugin in ImageJ, showing the correlation between NBD and mRuby3 fluorescence intensities at corresponding pixels. Normalized mean deviation product (nMDP) which mathematically represents correlation between intensities of corresponding pixels (values are ranging from -1 to 1). (B) GUVs were incubated with 0.6 μM mRuby3-CtAtg15 (73-475, S330A) at 25°C in pH4.0 buffer. (C) Particle size of filtered liposomes measured by Dynamic Light Scattering (DLS). Cumulant analysis results are shown. (D) Flotation assay using CtAtg15 (73-475, S330A) and indicated filtered liposomes.

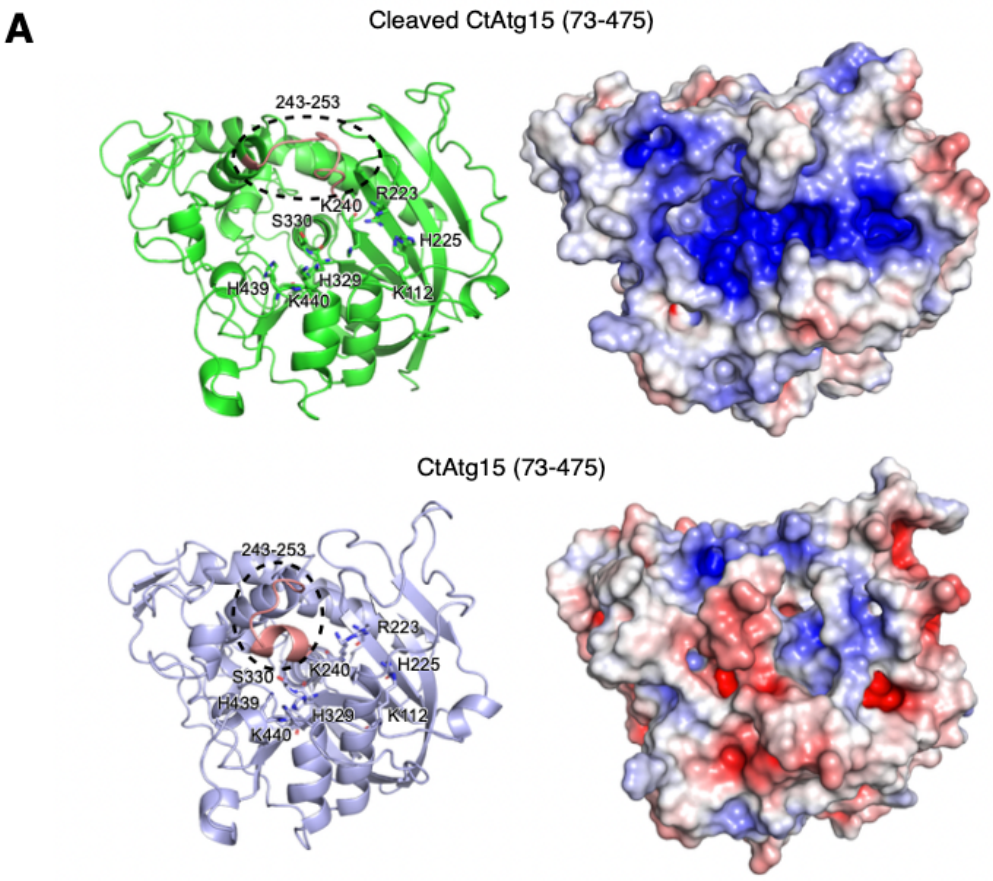
A
Cleaved CtAtg15 (73-475)
243-253
R223
K240
S330
H225
H439
H329
K112
K440
CtAtg15 (73-475)
243-253
R223
S330
K240
H225
H439
H329
K112
K440

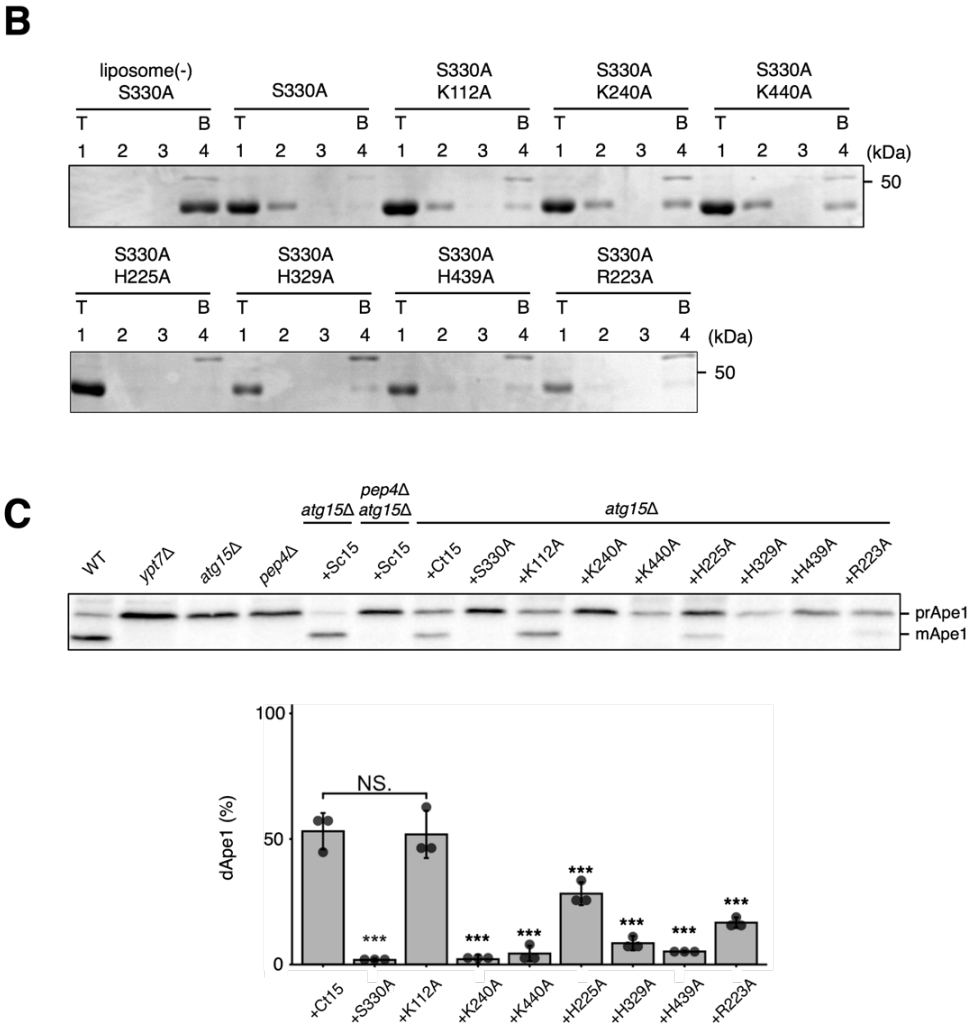

Fig. 6　Basic amino acids residues around the active center in CtAtg15

(A) Conformational change of CtAtg15 (73-475) predicted by MD simulation (Watanabe et al., 2023). The models on the left illustrate the positional relationships within the protein, with K112, R223, H225, K240, H329, H439, K440, and the active center S330 displayed in a ball-and-stick format. Amino acid residues 243–253 are colored in salmon pink and highlighted with dashed circles. The surface models on the right illustrate surface charge distribution (red indicates more negatively charged, blue indicates more positively charged). (B) Flotation assay using CtAtg15 (73-475, S330A) carrying the indicated mutations. (C) *S. cerevisiae* cells harboring indicated plasmids were cultured to 2.0×10^7 cells/ml in SD/CA medium and cell lysates were prepared by the alkaline lysis method. Western blot analysis was performed using anti-Ape1 antisera. Error bars indicate standard deviations. Statistical significance was determined using R (ver. 4.2.3) with one-way ANOVA followed by the Tukey–Kramer post hoc test. Data shown are representative of three independent experiments. N.S. indicates not significant. *P < 0.05, **P < 0.01, ***P < 0.001

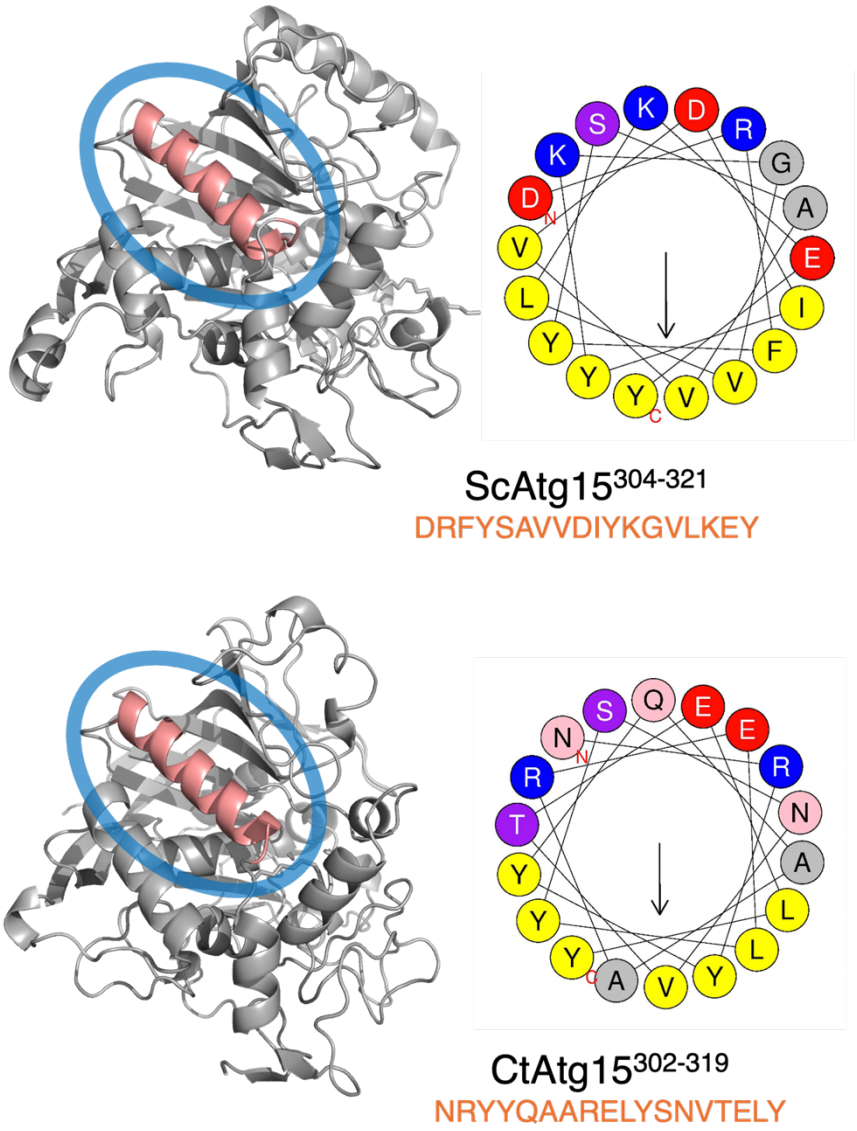

Fig. 7　The potential amphipathic lipid packing sensor (ALPS) motif

Each of the potential ALPS motifs and sequences for ScAt15 and CtAtg15, is presented. The potential ALPS motifs (salmon pink) were visualized in their corresponding structures (gray) predicted by Alphafold3 and are highlighted by blue circles. The helical-wheel representations of the potential ALPS motifs were analyzed using the HeliQuest web server and are shown, with an arrow in the center of each helical wheel indicating the direction and strength of the mean hydrophobic moment of the corresponding ALPS motif.

Acknowledgments

I would like to thank Dr. Yasunori Watanabe at Yamagata University for sharing expression plasmids with us.

I would like to thank Dr. Nozomu Kono and Mr. Sasuga Tanoue at The University of Tokyo for the advice about the GUV experiment.

I would like to thank Dr. Makiya Nishikawa and Ms. Mai Kanai at Tokyo University of Science for helping us measure the particle size of liposomes.